ELSEVIER

Where do inertial particles go in fluid flows?

George Haller*, Themistoklis Sapsis

Department of Mechanical Engineering, Massachusetts Institute of Technology, 77 Massachusetts Ave., Cambridge, MA 02139, USA

Abstract

We derive a general reduced-order equation for the asymptotic motion of finite-size particles in unsteady fluid flows. Our *inertial equation* is a small perturbation of passive fluid advection on a globally attracting slow manifold. Among other things, the inertial equation implies that particle clustering locations in two-dimensional steady flows can be described rigorously by the Q parameter, i.e., by one-half of the squared difference of the vorticity and the rate of strain. Use of the inertial equation also enables us to solve the numerically ill-posed problem of source inversion, i.e., locating initial positions from a current particle distribution. We illustrate these results on inertial particle motion in the Jung–Tél–Ziemniak model of vortex shedding behind a cylinder in crossflow.

1. Introduction

Finite-size or inertial particle dynamics in fluid flows can differ markedly from infinitesimal particle dynamics: both clustering and dispersion are well-documented phenomena in inertial particle motion, while they are absent in the incompressible motion of infinitesimal particles. As we show in this paper, these peculiar asymptotic features are governed by a lower-dimensional inertial equation which we determine explicitly.

Let $\mathbf{u}(\mathbf{x}, t)$ denote the velocity field of a two- or three-dimensional fluid flow of density ρ_f, with $\mathbf{x}$ referring to spatial locations and t denoting time. The fluid fills a compact (possibly time-varying) spatial region $\mathcal{D}$ with boundary $\partial \mathcal{D}$; we assume that $\mathcal{D}$ is a uniformly bounded smooth manifold for all times. We also assume $\mathbf{u}(\mathbf{x}, t)$ to be r times continuously differentiable in its arguments for some integer $r \geq 1$. We denote the material derivative of $\mathbf{u}$ by

$$\frac{D\mathbf{u}}{Dt} = \mathbf{u}_t + (\nabla \mathbf{u})\mathbf{u},$$

where ∇ denotes the gradient operator with respect to $\mathbf{x}$.

Let $\mathbf{x}(t)$ denote the path of a finite-size particle of density ρ_p immersed in the fluid. If the particle is spherical, its velocity $\mathbf{v}(t) = \dot{\mathbf{x}}(t)$ satisfies the equation of motion (cf. Maxey and Riley [13] and Babiano et al. [2])

$$
\begin{aligned}
\rho_p \dot{\mathbf{v}} = {} & \rho_f \frac{D\mathbf{u}}{Dt} \\
& + (\rho_p - \rho_f)\mathbf{g} \\
& - \frac{9\nu\rho_f}{2a^2}\left(\mathbf{v} - \mathbf{u} - \frac{a^2}{6}\Delta\mathbf{u}\right) \\
& - \frac{\rho_f}{2}\left[\dot{\mathbf{v}} - \frac{D}{Dt}\left(\mathbf{u} + \frac{a^2}{10}\Delta\mathbf{u}\right)\right] \\
& - \frac{9\rho_f}{2a}\sqrt{\frac{\nu}{\pi}}\int_0^t \frac{1}{\sqrt{t-s}}\left[\dot{\mathbf{v}}(s) - \frac{\mathrm{d}}{\mathrm{d}s}\left(\mathbf{u} + \frac{a^2}{6}\Delta\mathbf{u}\right)_{\mathbf{x}=\mathbf{x}(s)}\right]\mathrm{d}s.
\end{aligned}
\tag{1}
$$

Here ρ_p and ρ_f denote the particle and fluid densities, respectively, a is the radius of the particle, $\mathbf{g}$ is the constant vector of gravity, and ν is the kinematic viscosity of the fluid. The individual force terms listed in separate lines on the right-hand side of (2) have the following physical meaning: (1) force exerted on the particle by the undisturbed flow, (2) buoyancy force, (3) Stokes drag, (4) added mass term resulting

* Corresponding author. Tel.: +1 617 452 3064.
  E-mail address: ghaller@mit.edu (G. Haller).

from part of the fluid moving with the particle, and (5) the Basset–Boussinesq memory term. The terms involving $a^2 \Delta \mathbf{u}$ are usually referred to as the Fauxén corrections.

For simplicity, we assume that the particle is very small ($a \ll 1$), in which case the Fauxén corrections are negligible. We note that the coefficient of the Basset–Boussinesq memory term is equal to the coefficient of the Stokes drag term times $a/\sqrt{\pi \nu}$. Therefore, assuming that $a/\sqrt{\nu}$ is also very small, we neglect the last term in (2), following common practice in the related literature (Michaelides [14]). We finally rescale space, time, and velocity by a characteristic length scale L, characteristic time scale $T = L/U$ and characteristic velocity U, respectively, to obtain the simplified equations of motion

$$\dot{\mathbf{v}} - \frac{3R}{2} \frac{D\mathbf{u}}{Dt} = -\mu (\mathbf{v} - \mathbf{u}) + \left(1 - \frac{3R}{2}\right) \mathbf{g}, \qquad (2)$$

with

$$R = \frac{2\rho_f}{\rho_f + 2\rho_p}, \qquad \mu = \frac{R}{St}, \qquad St = \frac{2}{9} \left(\frac{a}{L}\right)^2 Re,$$

and with t, $\mathbf{v}$, $\mathbf{u}$ and $\mathbf{g}$ now denoting nondimensional variables. Variants of Eq. (2) have been studied by Babiano, Cartwright, Piro and Provenzale [2], Benczik, Toroczkai and Tél [5], and Vilela, de Moura and Grebogi [20].

In Eq. (2), St denotes the particle Stokes number and $Re = UL/\nu$ is the Reynolds number. The density ratio R distinguishes neutrally buoyant particles ($R = 2/3$) from aerosols ($0 < R < 2/3$) and bubbles ($2/3 < R < 2$). In the limit of infinitely heavy particles ($R = 0$), Eq. (2) become the Maxey–Riley equations derived originally in [13]. The $3R/2$ coefficient represents the added mass effect: an inertial particle brings into motion a certain amount of fluid that is proportional to half of its mass. For neutrally buoyant particles, the equation of motion is simply $\frac{D}{Dt} (\mathbf{v} - \mathbf{u}) = -\mu (\mathbf{v} - \mathbf{u})$, i.e., the relative acceleration of the particle is equal to the Stokes drag acting on the particle.

Rubin, Jones and Maxey [17] studied (2) with $R = 0$ in the special case when $\mathbf{u}$ describes a two-dimensional cellular steady flow model. They used a geometric singular perturbation approach developed by Fenichel [8] to understand particle settling in the flow. The same technique was employed by Burns et al. [7] in the study of particle focusing in the wake of a two-dimensional bluff body flow, which is steady in a frame co-moving with the von Kármán vortex street. Recently, Mograbi and Bar-Ziv [15] discussed this approach for general steady velocity fields and made observations about the possible asymptotic behaviors in two dimensions.

Here we consider finite-size particle motion in general unsteady velocity fields, extending Fenichel's geometric approach from time-independent to time-dependent vector fields. Such an extension has apparently not been considered before in dynamical systems theory, thus the present work should be of interest in other applications of singular perturbation theory where the governing equations are non-autonomous. We construct an attracting slow manifold that governs the asymptotic behavior of particles in system (2). We also obtain an explicit dissipative equation, the *inertial*

equation, that describes the flow on the slow manifold. This equation has half the dimension of the Maxey–Riley equation; this fact simplifies both the qualitative analysis of inertial dynamics and the numerical tracking of finite-size particles.

For two-dimensional steady flows, we use the inertial equation to give a complete description of the asymptotic behavior of aerosols, bubbles, and neutrally buoyant particles. For general unsteady flows, we show how the inertial equation can be used to locate the initial positions of dispersed particles. Such *source inversion* is not possible using the full Maxey–Riley equation, because for $\mu \gg 1$, the $-\mu \mathbf{u}$ term in (2) causes numerical solutions to blow up quickly in backward time. We illustrate the forward- and backward-time use of the inertial equation on the von Kármán vortex-street model of Jung, Tél and Ziemniak [12].

2. Singular perturbation formulation

The derivation of the equation of motion (2) is only correct under the assumption $\mu \gg 1$, which motivates us to introduce the small parameter

$$\epsilon = \frac{1}{\mu} \ll 1,$$

and rewrite (2) as a first-order system of differential equations:

$$\dot{\mathbf{x}} = \mathbf{v},$$

$$\epsilon \dot{\mathbf{v}} = \mathbf{u}(\mathbf{x}, t) - \mathbf{v} + \epsilon \frac{3R}{2} \frac{D\mathbf{u}(\mathbf{x}, t)}{Dt} + \epsilon \left(1 - \frac{3R}{2}\right) \mathbf{g}. \qquad (3)$$

This formulation shows that $\mathbf{x}$ is a slow variable changing at $\mathcal{O}(1)$ speeds, while the fast variable $\mathbf{v}$ varies at speeds of $\mathcal{O}(1/\epsilon)$.

To transform the above singular perturbation problem to a regular perturbation problem, we select an arbitrary initial time t_0 and introduce the fast time τ by letting

$$\epsilon \tau = t - t_0.$$

This type of rescaling is standard in singular perturbation theory with $t_0 = 0$. The new feature here is the introduction of a nonzero present time t_0 about which we introduce the new fast time τ. This trick enables us to extend the existing singular perturbation techniques to unsteady flows.

Denoting differentiation with respect to τ by prime, we rewrite (3) as

$$\mathbf{x}' = \epsilon \mathbf{v},$$

$$\phi' = \epsilon,$$

$$\mathbf{v}' = \mathbf{u}(\mathbf{x}, \phi) - \mathbf{v} + \epsilon \frac{3R}{2} \frac{D\mathbf{u}(\mathbf{x}, \phi)}{Dt} + \epsilon \left(1 - \frac{3R}{2}\right) \mathbf{g}, \qquad (4)$$

where $\phi \equiv t_0 + \epsilon \tau$ is a dummy variable that renders the above system of differential equations autonomous in the variables $(\mathbf{x}, \phi, \mathbf{v}) \in \mathcal{D} \times \mathbb{R} \times \mathbb{R}^n$; here n is the dimension of the domain of definition $\mathcal{D}$ of the fluid flow ($n = 2$ for planar flows, and $n = 3$ for three-dimensional flows).
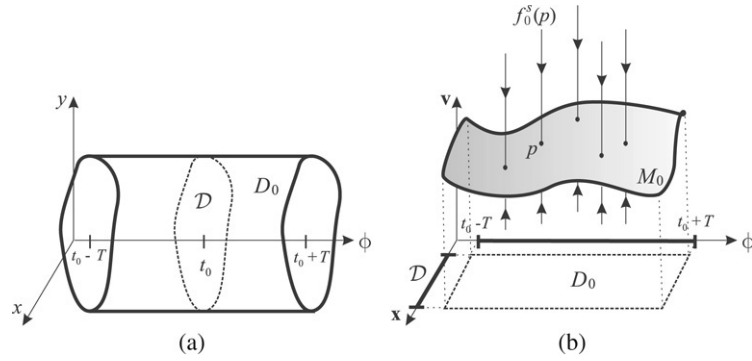
Fig. 1. (a) The geometry of the domain D_0. (b) The attracting set of fixed points M_0; each point p in M_0 has an n-dimensional stable manifold $f_0^s(p)$ (unperturbed stable fiber at p) satisfying $(\mathbf{x}, \phi) = const$.
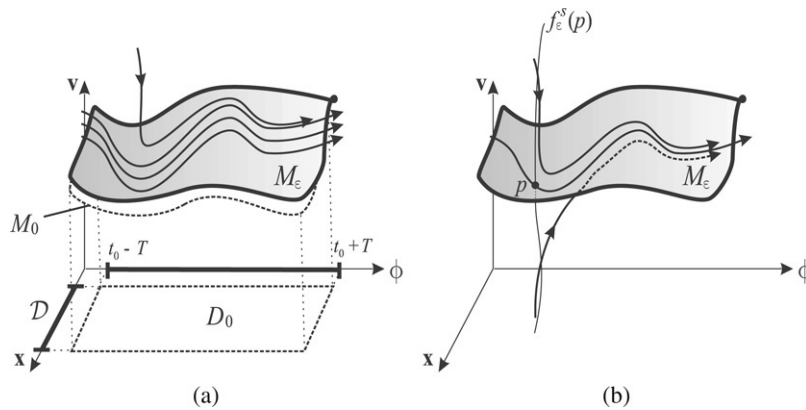

Fig. 2. (a) The geometry of the slow manifold M_ϵ. (b) A trajectory intersecting a stable fiber $f_\epsilon^s(p)$ converges to the trajectory through the fiber base point p.

3. Slow manifold and inertial equation

The $\epsilon = 0$ limit of system (4),

$$\mathbf{x}' = \mathbf{0},$$
$$\phi' = 0, \tag{5}$$
$$\mathbf{v}' = \mathbf{u}(\mathbf{x}, \phi) - \mathbf{v},$$

has an $n + 1$-parameter family of fixed points satisfying $\mathbf{v} = \mathbf{u}(\mathbf{x}, \phi)$. More formally, for any time $T > 0$, the compact invariant set

$$M_0 = \{(\mathbf{x}, \phi, \mathbf{v}) : \mathbf{v} = \mathbf{u}(\mathbf{x}, \phi), \mathbf{x} \in \mathcal{D}, \phi \in [t_0 - T, t_0 + T]\}$$

is completely filled with fixed points of (5). Note that M_0 is a graph over the compact domain

$$D_0 = \{(\mathbf{x}, \phi) : \mathbf{x} \in \mathcal{D}, \phi \in [t_0 - T, t_0 + T]\};$$

we show the geometry of D_0 and M_0 in Fig. 1.

Inspecting the Jacobian

$$\frac{d}{d\mathbf{v}} [\mathbf{u}(\mathbf{x}, \phi) - \mathbf{v}]_{M_0} = -\mathbf{I}_{n \times n},$$

we find that M_0 attracts nearby trajectories at a uniform exponential rate of $\exp(-\tau)$ (i.e., $\exp(-t/\epsilon)$ in terms of the original unscaled time). In fact, M_0 attracts all the solutions of (5) that satisfy $(\mathbf{x}(0), \phi(0)) \in \mathcal{D} \times [t_0 - T, t_0 + T]$; this can be verified

using the last equation of (5), which is explicitly solvable for any constant value of $\mathbf{x}$ and ϕ. Consequently, M_0 is a compact normally hyperbolic invariant set that has an open domain of attraction. Note that M_0 is not a manifold because its boundary

$$\partial M_0 = \partial \mathcal{D} \times [t_0 - T, t_0 + T] \bigcup \mathcal{D} \times \{t_0 - T\}$$
$$\bigcup \mathcal{D} \times \{t_0 + T\}$$

has corners; $M_0 - \partial M_0$, however, is an $n + 1$-dimensional normally hyperbolic invariant manifold.

By the results of Fenichel [8] for autonomous systems, any compact normally hyperbolic set of fixed points on (5) gives rise to a nearby locally invariant manifold for system (4). (Local invariance means that trajectories can only leave the manifold through its boundary.) In our context, Fenichel's results guarantee the existence of $\epsilon_0 (t_0, T) > 0$, such that for all $\epsilon \in [0, \epsilon_0)$, system (4) admits an attracting locally invariant manifold M_ϵ that is $\mathcal{O}(\epsilon)C^r$-close to M_0 (see Fig. 2). The manifold M_ϵ can be written in the form of a Taylor expansion

$$M_\epsilon = \left\{ (\mathbf{x}, \phi, \mathbf{v}) : \mathbf{v} = \mathbf{u}(\mathbf{x}, \phi) + \epsilon \mathbf{u}^1(\mathbf{x}, \phi) + \cdots \right.$$
$$\left. + \epsilon^r \mathbf{u}^r(\mathbf{x}, \phi) + \mathcal{O}(\epsilon^{r+1}), (\mathbf{x}, \phi) \in D_0 \right\}; \tag{6}$$

the functions $\mathbf{u}^k(\mathbf{x}, \phi)$ are as smooth as the right-hand side of (3). M_ϵ is a *slow manifold*, because (4) restricted to M_ϵ is a

slowly varying system of the form

$$\mathbf{x}' = \epsilon \mathbf{v}|_{M_\epsilon}$$
$$= \epsilon \left[\mathbf{u}(\mathbf{x}, \phi) + \epsilon \mathbf{u}^1(\mathbf{x}, \phi) + \cdots + \epsilon^r \mathbf{u}^r(\mathbf{x}, \phi) + \mathcal{O}(\epsilon^{r+1}) \right].$$
(7)

We find the functions $\mathbf{u}^k(\mathbf{x}, \phi)$ using the invariance of M_ϵ, which allows us to differentiate the equation defining M_ϵ in (6) with respect to τ. Specifically, differentiating

$$\mathbf{v} = \mathbf{u}(\mathbf{x}, \phi) + \sum_{k=1}^{r} \epsilon^k \mathbf{u}^k(\mathbf{x}, \phi) + \mathcal{O}(\epsilon^{r+1})$$

with respect to τ gives

$$\mathbf{v}' = \mathbf{u_x} \mathbf{x}' + \mathbf{u}_\phi \phi' + \sum_{k=1}^{r} \epsilon^k \left[\mathbf{u}_\mathbf{x}^k \mathbf{x}' + \mathbf{u}_\phi^k \phi' \right] + \mathcal{O}(\epsilon^{r+1}),$$
(8)

on M_ϵ, while restricting the $\mathbf{v}$ equations in (3) to M_ϵ gives

$$\mathbf{v}' = \left[\mathbf{u} - \mathbf{v} + \epsilon \frac{3R}{2} \frac{D\mathbf{u}}{Dt} + \epsilon \left(1 - \frac{3R}{2} \right) \mathbf{g} \right]_{M_\epsilon}$$
$$= -\sum_{k=1}^{r} \epsilon^k \mathbf{u}^k(\mathbf{x}, \phi) + \epsilon \frac{3R}{2} \frac{D\mathbf{u}}{Dt} + \epsilon \left(1 - \frac{3R}{2} \right) \mathbf{g}.$$
(9)

Comparing terms containing equal powers of ϵ in (8) and (9), then passing back to the original time t, we obtain the following result.

Theorem 1. *For small $\epsilon > 0$, the equation of particle motion (7) on the slow manifold M_ϵ can be rewritten as*

$$\dot{\mathbf{x}} = \mathbf{u}(\mathbf{x}, t) + \epsilon \mathbf{u}^1(\mathbf{x}, t) + \cdots + \epsilon^r \mathbf{u}^r(\mathbf{x}, t) + \mathcal{O}(\epsilon^{r+1}),$$
(10)

where r is an arbitrary but finite integer, and the functions $\mathbf{u}^i(\mathbf{x}, t)$ are given by

$$\mathbf{u}^1 = \left(\frac{3R}{2} - 1 \right) \left[\frac{D\mathbf{u}}{Dt} - \mathbf{g} \right],$$
$$\mathbf{u}^k = - \left[\frac{D\mathbf{u}^{k-1}}{Dt} + (\nabla \mathbf{u}) \mathbf{u}^{k-1} + \sum_{i=1}^{k-2} \left(\nabla \mathbf{u}^l \right) \mathbf{u}^{k-l-1} \right],$$
$$k \geq 2.$$
(11)

We shall refer to (10) with the $\mathbf{u}^i(\mathbf{x}, t)$ defined in (11) as the *inertial equation* associated with the velocity field $\mathbf{u}(\mathbf{x}, t)$, because (10) gives the general asymptotic form of inertial particle motion induced by $\mathbf{u}(\mathbf{x}, t)$. A leading-order approximation to the inertial equations is given by

$$\dot{\mathbf{x}} = \mathbf{u}(\mathbf{x}, t) + \epsilon \left(\frac{3R}{2} - 1 \right) \left[\frac{D\mathbf{u}(\mathbf{x}, t)}{Dt} - \mathbf{g} \right];$$
(12)

this is the lowest-order truncation of (10) that has nonzero divergence, and hence is capable of capturing clustering or dispersion arising from finite-size effects.

The above argument renders the slow manifold M_ϵ over the fixed time interval $[t_0 - T, t_0 + T]$. Since the choice of t_0 and T was arbitrary, we can extend the existence result of M_ϵ to an arbitrary long finite time interval.
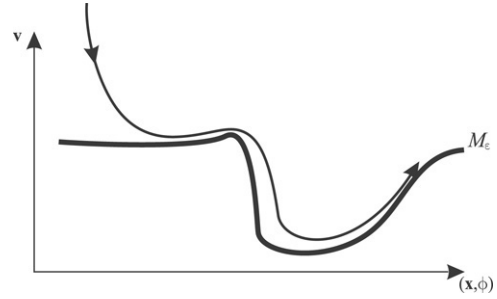

Fig. 3. Sudden changes in the velocity-field delay convergence to the slow manifold.

Slow manifolds are typically not unique, but obey the same asymptotic expansion (11). Consequently, any two slow manifolds and the corresponding inertial equations are $\mathcal{O}(\epsilon^r)$ close to each other. Specifically, if $r = \infty$, then the difference between any two slow manifolds is exponentially small in ϵ. The case of neutrally buoyant particles ($R = 2/3$) turns out to be special: the slow manifold is the unique invariant surface

$$M_\epsilon = \{ (\mathbf{x}, \phi, \mathbf{v}) : \mathbf{v} = \mathbf{u}(\mathbf{x}, \phi), (\mathbf{x}, \phi) \in D_0 \},$$

on which the dynamics coincides with those of infinitesimally small particles. This invariant surface survives for arbitrary $\epsilon > 0$, as noticed by Babiano et al. [2], but may lose its stability for larger values of ϵ (cf. Sapsis and Haller [18]).

4. Convergence to the slow manifold

The results of Fenichel [8] guarantee exponential convergence of solutions of (4) to the slow manifold M_ϵ. Translated to the original variables, exponential convergence with a uniform exponent to the slow manifold is only guaranteed over the compact time interval $[t_0 - T, t_0 + T]$.

Over finite time intervals, exponentially dominated convergence is not necessarily monotone. For instance, if the velocity field suddenly changes, say, at speeds comparable to $\mathcal{O}(1/\epsilon)$, then converged solutions may suddenly find themselves again at an increased distance from the slow manifold before they start converging again (cf. Fig. 3). Again, this is the consequence of the lack of compactness in time, which results in a lack of uniform exponential convergence to the slow manifold over infinite times.

Where do solutions converging to the slow manifold tend asymptotically? Observe that for $\epsilon = 0$, each solution converging to M_0 is confined to an n-dimensional plane

$$f_0^s(p) = \left\{ (\mathbf{x}_p, \phi_p, \mathbf{v}) : p = (\mathbf{x}_p, \phi_p, \mathbf{u}(\mathbf{x}_p, \phi_p)) \in M_0 \right\}.$$

Fenichel refers to $f_0^s(p)$ as the *stable fiber* associated with the point p: each trajectory in $f_0^s(p)$ converges to the base point of the fiber, p. More generally, a stable fiber has the property that each solution intersecting the fiber converges exponentially in time to the solution passing through the base point of the fiber. The collection of all fibers intersecting M_0 is called the stable foliation of M_0, or simply the stable manifold of M_0.

Fenichel [8] showed that the stable foliation of M_0 smoothly persists for small enough $\epsilon > 0$. Specifically, associated with

each point $p \in M_\epsilon$, there is an n-dimensional manifold $f_\epsilon^s(p)$ such that any solution of (4) intersecting $f_\epsilon^s(p)$ will converge at an exponential rate to the solution that runs through the point p on M_ϵ. The persisting stable fibers $f_\epsilon^s(p)$ are C^r smooth in ϵ, hence they are $\mathcal{O}(\epsilon)C^r$-close to the invariant planes $f_0^s(p)$, as indicated in Fig. 2(b).

5. Use of the slow manifold and inertial equation

5.1. Asymptotics of finite-size particle motion

A general particle motion $(\mathbf{x}(t), \mathbf{v}(t))$ is attracted to a specific solution within the slow manifold M_ϵ. This specific solution runs through the base points of stable fibers intersected by $(\mathbf{x}(t), \mathbf{v}(t))$. As a result, the forward-time asymptotic behaviors seen on the slow manifold are the only possible asymptotic behaviors for general inertial particle motion.

Rapid changes in the velocity field $\mathbf{u}(\mathbf{x}, t)$ in time will lead to rapid changes in the slow manifold, as seen from the definition of M_ϵ in (6). In that case, particles that have already converged to the slow manifold may find themselves further away from the slow manifold (whose location has rapidly changed). Particles will converge exponentially to the new location of the slow manifold, but may again find themselves temporarily at a large distance from the manifold if a further rapid change occurs in the velocity field.

5.2. Source inversion: Tracing particles in backward time

Finding a localized source of particle release based on later observation of the particles is of interest in several applications. Such a source-inversion problem appears, for instance, in locating the source of airborne or waterborne pollution from the observations of a dispersed pollutant (Akcelik et al. [1], Boano et al. [6], Badia et al. [3], Katopodes Chow et al. [11]). In such applications, locating the source involves approximating the ill-posed backward-time solution of the appropriate advection–diffusion equation.

Even without diffusion, however, source-inversion for finite-size particles is challenging. Technically speaking, the equations of motion (4) are well-posed in backward time: they have unique solutions with continuous dependence on initial data. Nevertheless, (4) generates strong exponential growth with exponent $1/\epsilon$ for decreasing t. This strong instability leads to an inevitable and speedy numerical blowup in backward-time integration.

By contrast, the inertial equation (10) is free from the above instability, and hence can be solved in backward time without difficulty. This enables us to recover the starting position $\mathbf{x}(t_0)$ of any solution $(\mathbf{x}(t), \mathbf{v}(t))$ as follows.

Theorem 2. Let $\varphi(t; t_0, \mathbf{x}_0)$ denote at time t the solution of the inertial equation (10) that starts from $\mathbf{x}_0$ at time t_0. Let $(\mathbf{x}(t; t_0, \mathbf{x}_0, \mathbf{v}_0), \mathbf{v}(t; t_0, \mathbf{x}_0, \mathbf{v}_0))$ denote at time t the solution of the full Maxey–Riley equation (3) that starts from $(\mathbf{x}_0, \mathbf{v}_0)$ at time t_0. Then for any fixed $(\mathbf{x}_0, \mathbf{v}_0)$ and for small enough $\epsilon > 0$, we have

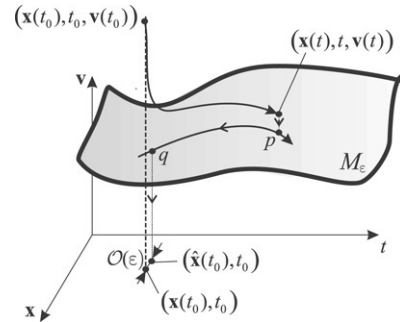$$|\varphi(t_0; t, \mathbf{x}(t; t_0, \mathbf{x}_0, \mathbf{v}_0)) - \mathbf{x}_0| = \mathcal{O}(\epsilon).$$

Fig. 4. Source inversion for inertial particles using the slow manifold.

In other words, at any time t, we can recover the starting position $\mathbf{x}_0$ of an inertial particle by first projecting the corresponding solution of (3) onto the slow manifold along the $\mathbf{v}$ direction, then solving the inertial equation (10) backwards from time t to t_0. This procedure leads to a point $\hat{\mathbf{x}}(t_0) = \varphi(t_0; t, \mathbf{x}(t; t_0, \mathbf{x}_0, \mathbf{v}_0))$ that is $\mathcal{O}(\epsilon)$ close to the starting point $\mathbf{x}_0$ (cf. Fig. 4).

Proof. Our projection onto the slow manifold takes place along the $(\,\cdot\,, t, \mathbf{x}(t))$ subspace, i.e., along an unperturbed stable fiber through the point $(\mathbf{x}(t; t_0, \mathbf{x}_0, \mathbf{v}_0), t, \mathbf{v}(t; t_0, \mathbf{x}_0, \mathbf{v}_0))$. Therefore, by the smoothness of fibers in ϵ, the resulting projected point p on M_ϵ is $\mathcal{O}(\epsilon)$ close to the base point $\hat{p}$ of the stable fiber $f_\epsilon^s(\hat{p})$ that contains $(\mathbf{x}(t; t_0, \mathbf{x}_0, \mathbf{v}_0), t, \mathbf{v}(t; t_0, \mathbf{x}_0, \mathbf{v}_0))$. Let $q = (\hat{\mathbf{x}}(t_0), \hat{\mathbf{v}}(t_0))$ be the point on the slow manifold that we obtain by following the solution through the point p from time t backwards to time t_0. Note that $\hat{\mathbf{x}}(t_0) = \varphi(t_0; t, \mathbf{x}(t; t_0, \mathbf{x}_0, \mathbf{v}_0))$. By the invariance and smoothness of the stable fiber family, the fiber $f_\epsilon^s(q)$ will be $\mathcal{O}(\epsilon)\ C^{r-1}$ close to $f_\epsilon^s(q^*)$, the fiber containing the initial condition $(\mathbf{x}(t_0), t_0, \mathbf{v}(t_0))$. Since $f_\epsilon^s(q^*)$ is in turn $\mathcal{O}(\epsilon)\ C^{r-1}$ close to an unperturbed stable fiber (the n-dimensional $\mathbf{v}$-plane running through q^*), we conclude that $(\hat{\mathbf{x}}(t_0), t_0)$, the $(\mathbf{x}, t)$-projection of q, is $\mathcal{O}(\epsilon)$-close to $(\mathbf{x}(t_0), t_0)$. Therefore, backward-integration after projection onto the slow manifold recovers the initial condition of a trajectory with $\mathcal{O}(\epsilon)$ error. Note that the initial velocity $\mathbf{v}(t_0)$ is not recovered by this procedure. $\quad\square$

6. Special case: Inertial particles in two-dimensional steady flows

For $0 < \epsilon \ll 1$, all finite-size particle trajectories tend exponentially fast to the slow manifold. As a result, asymptotic particle behavior in steady flows is governed by the steady inertial equation

$$\dot{\mathbf{x}} = \mathbf{u}(\mathbf{x}) + \epsilon \mathbf{u}^1(\mathbf{x}) + \cdots + \epsilon^r \mathbf{u}^r(\mathbf{x}) + \mathcal{O}(\epsilon^{r+1}), \tag{13}$$

where the functions $\mathbf{u}^k$ defined in (11) are computed from the steady velocity field $\mathbf{u}(\mathbf{x})$.

Eq. (13) is an autonomous ordinary differential equation (ODE) for the particle trajectory $\mathbf{x}(s)$. The qualitative theory of such ODEs is fairly complete in the two-dimensional case; this fact leads to powerful general conclusions about the asymptotics of finite-size particle dynamics in two-dimensional flows. The results derived below use the inertial equation to

make specific predictions about inertial particle motion in two-dimensional steady flows (see also Mograbi and Bar-Ziv [15] for some general observations about the same subject).

Let us first define the quantity

$$Q(\mathbf{x}, t) = \frac{1}{2} \left(|\boldsymbol{\Omega}(\mathbf{x}, t)|^2 - |\mathbf{S}(\mathbf{x}, t)|^2 \right), \tag{14}$$

with $|\cdot|$ denoting the Euclidean matrix norm, and with the vorticity tensor $\boldsymbol{\Omega}$ and the rate-of-strain tensor $\mathbf{S}$ defined as

$$\boldsymbol{\Omega} = \frac{1}{2} \left[\nabla \mathbf{u} - (\nabla \mathbf{u})^T \right], \qquad \mathbf{S} = \frac{1}{2} \left[\nabla \mathbf{u} + (\nabla \mathbf{u})^T \right]. \tag{15}$$

For later use, we also define a specially weighted average of the of Q along a closed streamline Γ_0 of the velocity field $\mathbf{u}(\mathbf{x})$:

$$I(\Gamma_0) = \int_{\Gamma_0} \frac{(2 - 3R) Q}{|\mathbf{u}|} \, \mathrm{d}s.$$

Finally, we denote the interior of Γ_0 by $\mathrm{Int}(\Gamma_0)$.

We note that Q, the second scalar invariant of the velocity gradient $\nabla \mathbf{u}$, is broadly used as an indicator of the stability of two-dimensional fluid particle motion. Specifically, the Okubo–Weiss criterion (Okubo [16], Weiss [19]) identifies $Q > 0$ regions as elliptic (vortex-type) and $Q < 0$ regions as hyperbolic (saddle-type). This classification is based on ad hoc arguments that can only be justified near stagnation points of steady flows (Basdevant and Philipovitch [4]); away from such stagnation points, the criterion has been shown to be incorrect (Haller and Yuan [9]).

While ill-justified for infinitesimal particle motion, Q turns out to be a rigorous tool for predicting the asymptotic behavior of finite-size particles. Specifically, we have the following result.

Theorem 3. *For $\epsilon > 0$ small enough:*

(i) *A typical aerosol in a compact steady flow will converge to a closed curve Γ_ϵ that is $\mathcal{O}(\epsilon)$ C^1-close to a closed streamline Γ_0 of $\mathbf{u}(\mathbf{x})$. This Γ_0 satisfies*

$$\int_{\mathrm{Int}(\Gamma_0)} Q \, \mathrm{d}A = 0,$$
$$\int_{\mathrm{Int}(\Gamma_-)} Q \, \mathrm{d}A > 0 > \int_{\mathrm{Int}(\Gamma_+)} Q \, \mathrm{d}A \tag{16}$$

for all closed streamlines Γ_- and Γ_+ close enough to Γ_0 with the property $\mathrm{Int}(\Gamma_-) \subset \mathrm{Int}(\Gamma_0) \subset \mathrm{Int}(\Gamma_+)$. If Γ_0 contains no fixed points, then Γ_ϵ is stable limit cycle, and condition (16) is equivalent to

$$\int_{\mathrm{Int}(\Gamma_0)} Q \, \mathrm{d}A = 0, \quad I(\Gamma_0) < 0. \tag{17}$$

(ii) *A typical bubble in a compact steady flow will converge to either a center-type fixed point of (2) or a closed curve Γ_ϵ that is $\mathcal{O}(\epsilon)$ C^1-close to a closed streamline Γ_0 of $\mathbf{u}(\mathbf{x})$. This Γ_0 satisfies*

$$\int_{\mathrm{Int}(\Gamma_0)} Q \, \mathrm{d}A = 0,$$
$$\int_{\mathrm{Int}(\Gamma_-)} Q \, \mathrm{d}A < 0 < \int_{\mathrm{Int}(\Gamma_+)} Q \, \mathrm{d}A \tag{18}$$

for all closed streamlines Γ_- and Γ_+ close enough to Γ_0 with the property $\mathrm{Int}(\Gamma_-) \subset \mathrm{Int}(\Gamma_0) \subset \mathrm{Int}(\Gamma_+)$. If Γ_0 contains no fixed points, then Γ_ϵ is a stable limit cycle, and condition (18) is equivalent to

$$\int_{\mathrm{Int}(\Gamma_0)} Q \, \mathrm{d}A = 0, \quad I(\Gamma_0) > 0.$$

(iii) *A typical neutrally buoyant particle will converge to a streamline of $\mathbf{u}(\mathbf{x})$.*

(iv) *A saddle-type fixed point of the two-dimensional steady velocity field will act as a saddle for any finite-size particle motion (i.e., for aerosols, bubbles, and neutrally buoyant particles).*

Proof. See the Appendix. $\square$

The term *typical* in statements (i)–(iii) above is meant to exclude atypical trajectories that are in the stable manifold of a saddle fixed point of (10) and hence converge to that saddle.

7. Example: Inertial particles in the unsteady wake of a cylinder

7.1. Model flow

To illustrate our results, we consider inertial particle motion in the von Kármán vortex street model of Jung, Tél and Ziemniak [12]. Finite-size particle motion in this flow has already been studied numerically by Benczik, Toroczkai and Tél [5], who showed the existence of attractors for certain parameter values.

Assuming incompressibility for the vortex street, we have a stream function for the flow, which Jung, Tél and Ziemniak [12] assume in the form

$$\Psi(x, y, t) = f(x, y)g(x, y, t), \tag{19}$$

with

$$f(x, y) = 1 - \exp\left(-a^{-1/2} \left(\left(x^2 + y^2 \right)^{1/2} - 1 \right)^2 \right). \tag{20}$$

This form of $f(x, y)$ ensures the correct no-slip boundary behavior for the flow at the cylinder surface that satisfies $x^2 + y^2 = 1$. The coefficient $a^{-1/2}$ represents the width of the boundary layer. The factor g in (19) models the contributions of the shed vortices and the background flow u_0 to the full flow. More specifically,

$$g(x, y, t) = -wh_1(t)g_1(x, y, t) + wh_2(t)g_2(x, y, t) + u_0 ys(x, y). \tag{21}$$

The first two terms in (21) describe the alternating creation, evolution and damping of two vortices of equal strength. The quantities w and $h_i(t)$ represent the overall vortex strength and amplitudes, respectively. Because of the alternating nature of the vortices, we have a constant phase difference of half-period $T_c/2$ between the strength of the two vortices, i.e. $h_2(t) = h_1(t - T_c/2)$. To describe the time evolution of the vortex strengths, we choose
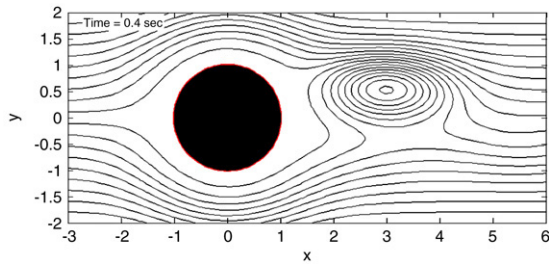
$$h_1(t) = |\sin(\pi t / T_c)|. \tag{22}$$

Fig. 5. Streamlines of the model flow at $t = 0.4$.

The vortex centers are assumed to move parallel to the x-axis at a constant speed, satisfying

$$x_1(t) = 1 + L\left[(t/T_c)\,\mathrm{mod}\,1\right], \qquad x_2(t) = x_1\left(t - T_c/2\right),$$
$$y_1(t) = -y_2(t) \equiv y_0.$$

The shape of the shed vortices is controlled by the factor

$$g_i(x, y, t) = \exp\left(-R_0\left[(x - x_i(t))^2 + \alpha^2(y - y_i(t))^2\right]\right),$$

where $R_0^{1/2}$ is the characteristic vortex size, and α is an aspect ratio parameter.

Finally, the last term in Eq. (21) represents the contribution of the background flow of uniform velocity u_0. The factor $s(x, t)$ is introduced in order to simulate the shielding of the background flow just behind the cylinder; it is taken to be of the form

$$s(x, y) = 1 - \exp\left(-(x - 1)^2/\alpha^2 - y^2\right).$$

As in Jung, Tél and Ziemniak [12], we choose a set of parameters for which the model has been shown to approximate the Navier–Stokes solution for this geometry with $Re \approx 250$. More specifically, we set the nondimensional parameter values $\alpha = 2, R_0 = 0.35, L = 2, a = 1$ and $y_0 = 2$. For the background flow velocity, we choose $u_0 = 14/T_c$, while the average strength of the vortices is taken to be $w = 8 \times 24/\pi$ as in Benczik, Toroczkai and Tél [5]. As shown by Jung, Tél and Ziemniak [12], the above set of parameters leads to a flow period of $T_c = 1.107$. We show a representative snapshot of the corresponding flow in Fig. 5.

7.2. Slow-manifold in the model flow

Here we show that the inertial equation (10) indeed gives the correct asymptotic motion of finite-size particles in this example. For particles, we choose bubbles with $R = 1.55$ and $\epsilon = 0.01$. Gravity is ignored in the model ($\mathbf{g} = \mathbf{0}$). First, we solve the full four-dimensional Maxey–Riley equation (3) on the time interval $[0, 1.12]$ using a fourth-order Runge–Kutta algorithm with absolute integration tolerance 10^{-7}. We release several bubbles with their initial spatial location taken from the grey circle shown in Fig. 6. The initial velocities of all particles were taken much larger in absolute value than the velocities corresponding to the same initial location on the slow manifold. In the same figure, we also show the projection of the four-dimensional solution of (3) onto the $\mathbf{x} = (x, y)$ plane. Note that all bubbles converge to the same attracting fluid trajectory.
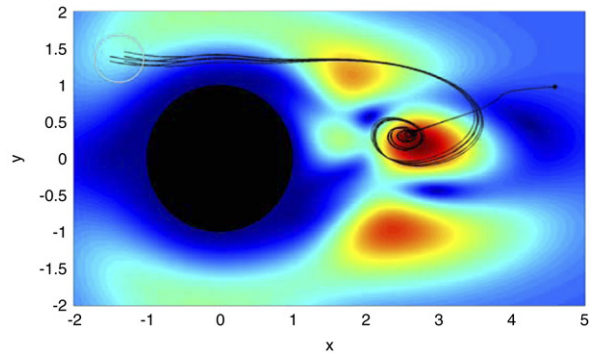

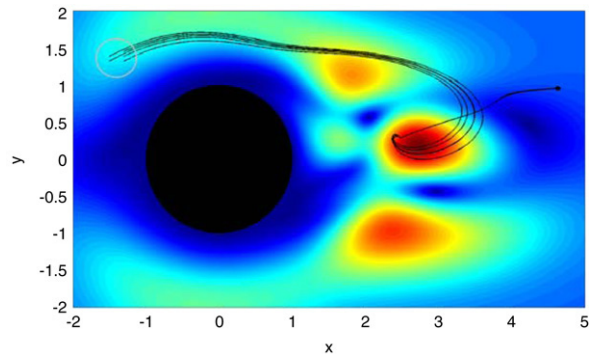Fig. 6. Simulated bubble motion in the full Maxey–Riley equations.

Fig. 7. Simulated bubble motion in the truncated inertial equation (12).

By contrast, Fig. 7 shows the dynamics on the slow manifold M_ϵ. To generate this picture, we used the same initial bubble locations on M_ϵ to solve the truncated inertial equation (12) over the same time interval. Over an initial period of exponentially fast decay to M_ϵ, the trajectories and their projections on the slow manifold only show qualitative similarities; the details of their geometries differ, especially while they pass through a moving vortex behind the cylinder. This is not surprising: even two very close initial positions on the slow manifold will generate noticeably different trajectories in regions with sensitive dependence on initial conditions.

In the present example, however, there exists a downstream moving attractor on the slow manifold (cf. Fig. 7). This attractor is a distinguished fluid trajectory that attracts all nearby inertial trajectories and hence ultimately eliminates sensitive dependence on initial conditions. Fig. 6 shows that solutions of the full Maxey–Riley equation also cluster around this time-varying attractor. By working on the slow manifold, we have reduced the dimension of the particle tracking problem from four to two, still reproducing the same asymptotic clustering behavior seen in the full Maxey–Riley equation.

Both in Figs. 6 and 7, we use color to indicate the instantaneous leading-order geometry of the slow manifold (6) at time $T = 1.2$. Specifically, colors ranging from dark blue to dark red indicate increasing values of $|\mathbf{v}| = |\mathbf{u}(\mathbf{x}, T)|$, which is a measure of the "height" of the slow manifold at leading order in the $(\mathbf{x}, \mathbf{v})$ coordinate space.
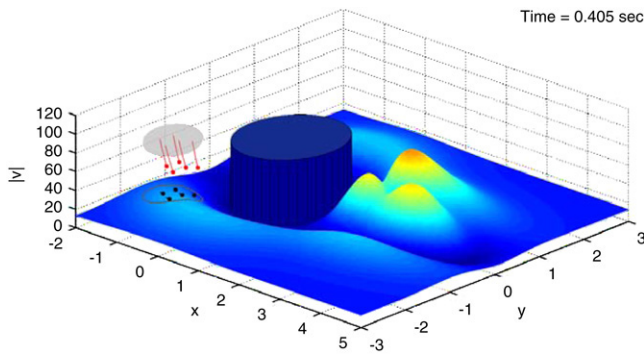
Fig. 8. Bubbles released and advected under the full Maxey–Riley equation (red curves). Particles with the same initial condition released and advected on the first-order approximation of the slow manifold under the truncated inertial equation (black curves). Both the cylinder and the approximate slow manifold are shown in the $(x, y, |\mathbf{v}|)$ space. (For interpretation of the references to colour in this figure legend, the reader is referred to the web version of this article.)
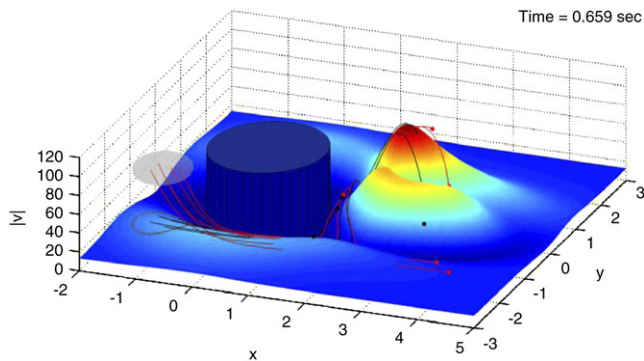

Fig. 9. Final dispersed positions of the full particle trajectories (red curves) and of their projections on the slow manifold (black curves). (For interpretation of the references to colour in this figure legend, the reader is referred to the web version of this article.)

7.3. Source inversion in the model flow

We now illustrate the use of the truncated inertial equation (12) in identifying initial positions of dispersed finite-size particles. Again, for particles, we choose bubbles with $R = 1.55$ and $\epsilon = 0.01$. We launch a set of of particles and track them using the full Maxey–Riley equation; we also track the evolution of the projected initial locations of the particles on the slow manifold. Once the particles have dispersed, we stop them and attempt to trace them back to their initial conditions by integrating the Maxey–Riley equation and the truncated inertial equations, respectively, in backward time (the maximal integration error tolerance is again 10^{-7} in the fourth-order Runge–Kutta scheme we use).

Almost immediately, the backward computations for the full Maxey–Riley equation blow up due to the numerical instability caused by the $-\mathbf{v}/\epsilon$ term. By contrast, the inertial equation on the slow manifold leads us back to the initial locations of the released particles. All this is documented in Figs. 8–10, where we track the forward and backward integration projected from the four-dimensional phase space of Eq. (3) to the space $(x, y, |\mathbf{v}|)$; we also graph the cylinder and the approximate slow manifold at select times.
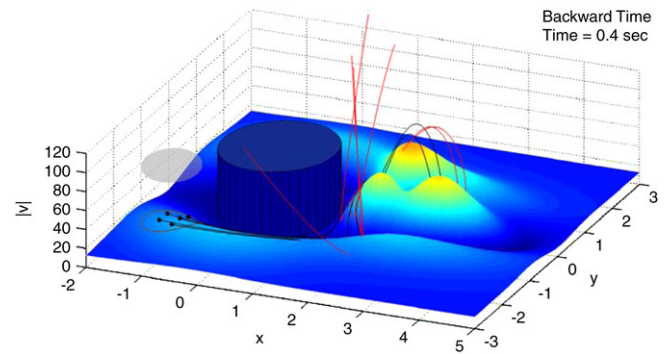

Fig. 10. Backward integration from the final dispersed positions. The full Maxey–Riley trajectories quickly blow up (red curves), while the truncated inertial equations on the slow manifold yield a correct approximation for the initial bubble locations (black curves). (For interpretation of the references to colour in this figure legend, the reader is referred to the web version of this article.)

8. Conclusions

In this paper, we have described a way to reduce the Maxey–Riley equation to a slow manifold that captures the asymptotics of inertial particle dynamics. The slow manifold arises in a singular perturbation approach that is valid for small particle Stokes numbers. We treat general unsteady flows, as opposed to earlier applications of singular perturbation theory in this context that were restricted to concrete steady flows.

Our main result is an explicit inertial equation for motions on the slow manifold. For small enough Stokes numbers, particles approach trajectories of this inertial equation exponentially fast. It is therefore enough to understand the asymptotic features of the inertial equation to understand the asymptotics of finite-size particle motion. We have also shown that the inertial equation can be used to tackle the numerically ill-posed problem of source inversion. Finally, we have obtained a full classification of possible asymptotic features of particle motion in steady two-dimensional flows. The classification is based on the Okubo–Weiss parameter Q, which (surprisingly) becomes a mathematically exact predictive tool once particles are not infinitesimally small. Specifically, we have derived formulae involving Q that predict the locations of particle clustering at points or along limit cycles.

We have illustrated the forward- and backward-time use of the inertial equation on the vortex-shedding model of Jung, Tél and Ziemniak [12]. Specifically, we have verified the accuracy of the slow-manifold approximation in forward time, and that of our proposed source-inversion technique in backward time.

Extension of our results on steady inertial motion from two to three-dimensions would be challenging since even three-dimensional steady flows can be nonintegrable. A natural candidate class for the extension is nondegenerate steady Euler flows that are known to be integrable. A further question of interest is how the stability of the slow manifold changes as the Stokes number is increased. Initial results in this direction for neutrally buoyant particles appear in the works of Babiano et al. [2] and Vilela et al. [20]. Specific results on instabilities along the slow manifold will appear in Sapsis and Haller [18].

Appendix. Proof of Theorem 3

A.1. Volume evolution in the inertial equation

For later use, we first compute the change of an infinitesimal volume $V(t)$ along a solution $\mathbf{x}(t)$ of (12). By Liouville's theorem, the volume $V(t)$ satisfies

$$
V(t) = V(t_0) \exp \left\{ \int_{t_0}^{t} \nabla \cdot \left[\mathbf{u}(\mathbf{x}, s) \right. \right.
$$
$$
\left. \left. + \epsilon \left(\frac{3R}{2} - 1 \right) \left[\frac{D\mathbf{u}(\mathbf{x}, s)}{Dt} - \mathbf{g} \right] \right]_{\mathbf{x}=\mathbf{x}(s)} ds \right\} \qquad (24)
$$

for any choice of the initial time t_0. In evaluating the above expression, we assume that the fluid flow is incompressible, which implies

$$
\nabla \cdot \mathbf{u} = 0,
$$
$$
\nabla \cdot \frac{\partial \mathbf{u}}{\partial t} = \frac{\partial}{\partial t} \nabla \cdot \mathbf{u} = 0,
$$
$$
\nabla \cdot [(\nabla \mathbf{u})\mathbf{u}] = \text{Trace}[\nabla \mathbf{u} \nabla \mathbf{u}] = -2Q, \qquad (25)
$$
$$
\nabla \cdot \mathbf{u}^1 = \nabla \cdot \left(\frac{3R}{2} - 1 \right) \left[\frac{D\mathbf{u}(\mathbf{x}, s)}{Dt} - \mathbf{g} \right] = (2 - 3R) \, Q,
$$

with Q defined in (14). Using (25), we rewrite the volume evolution formula (24) as

$$
V(t) = V(t_0) \exp \left\{ \epsilon \, (2 - 3R) \int_{t_0}^{t} Q(\mathbf{x}(s), s) ds \right\}. \qquad (26)
$$

A.2. Fixed points of the inertial equation

As a general rule for steady flows, fixed points of the velocity field $\mathbf{u}(\mathbf{x})$ are also fixed points of the inertial equation (10). This can be concluded from (11) by noting that $\mathbf{u}(\mathbf{x}_0) = 0$ implies $\mathbf{u}^k(\mathbf{x}_0) = 0$ for all $k \geq 1$. Also note that for small enough $\epsilon > 0$, a center-type fixed point of $\mathbf{u}$ becomes a center or a spiral of the inertial equation, because the right-hand-side of (10) is a small perturbation of $\mathbf{u}$. For the same reason, a saddle-type fixed point of $\mathbf{u}$ is a saddle-type fixed point of (10) for small $\epsilon > 0$, which proves the statement (iv) of Theorem 3.

To identify the stability of a spiral-type fixed point perturbing from a center-type fixed point of $\mathbf{u}$, we first recall that $Q > 0$ holds at elliptic fixed points (centers) of $\mathbf{u}$. If $\mathbf{x}(s) \equiv \mathbf{x}_0$ is a fixed point of the inertial equation, the time evolution of a infinitesimal volume $V(t_0)$ based at $\mathbf{x}_0$ can be computed from (26) as

$$
V(t) = V(t_0) \exp \left\{ \epsilon \, (2 - 3R) \, Q(\mathbf{x}_0) \, (t - t_0) \right\}.
$$

Therefore, if $\mathbf{x}_0$ is an elliptic fixed point of $\mathbf{u}(\mathbf{x})$ (i.e., $Q > 0$), then $V(t)$ grows for aerosols ($2 - 3R > 0$), and shrinks for bubbles ($2 - 3R < 0$). For neutrally buoyant particles, the perturbation terms to $\mathbf{u}$ on the right-hand side of (10) are all zero, therefore a center for $\mathbf{u}$ will remain a center for the inertial equation in the neutrally buoyant case. In summary: center of a two-dimensional steady velocity field will act as a source for aerosols, as a sink for bubbles, and as a center for neutrally buoyant particles.

A.3. Asymptotic dynamics on the slow manifold

Assume now that the steady velocity field $\mathbf{u}(\mathbf{x})$ is defined on a compact two-dimensional planar domain or on a two-dimensional surface diffeomorphic to a sphere. Then, the slow manifold M_ϵ, as a smooth graph over the domain of definition of $\mathbf{u}(\mathbf{x})$, is also a compact two-dimensional invariant manifold (with or without boundary). Applying the Poincaré–Bendixson theorem to M_ϵ, we conclude that all trajectories of (10) tend to a limit cycle, a fixed point, or to a set formed by fixed points and homoclinic or heteroclinic orbits connecting those fixed points. Since heteroclinic and homoclinic orbits are structurally unstable, we conclude that non-neutrally-buoyant particles in generic compact flows tend to fixed points or limit cycles.

Combining this last observation with the discussion above on fixed points of the inertial equation, we obtain the following conclusions:

A.3.1. Aerosols

Aerosols cannot cluster around fixed points: as we have seen above, fixed points for aerosol dynamics are unstable spirals or saddles, neither of which can create clustering. As a result, aerosols will cluster around closed curves S_ϵ that are either limit cycles, or connected sets composed of some combination of fixed points, homoclinic orbits, and heteroclinic orbits. For $\epsilon > 0$ small enough, such a closed curve Γ_ϵ is $\mathcal{O}(\epsilon) \, C^1$-closed to a closed streamline Γ_0 of the velocity field $\mathbf{u}(\mathbf{x})$.

The phase-space volume bounded by Γ_ϵ does not change in time, therefore

$$
\int_{\text{Int}(\Gamma_\epsilon)} \nabla \cdot \left[\mathbf{u}(\mathbf{x}) + \epsilon \mathbf{u}^1(\mathbf{x}) + \cdots + \epsilon^r \mathbf{u}^r(\mathbf{x}) + \mathcal{O}(\epsilon^{r+1}) \right] dV
$$
$$
= \epsilon \int_{\text{Int}(\Gamma_\epsilon)} \nabla \cdot \left[\mathbf{u}^1(\mathbf{x}) + \cdots + \epsilon^{r-1} \mathbf{u}^r(\mathbf{x}) + \mathcal{O}(\epsilon^r) \right] dV = 0.
$$

Dividing by ϵ, taking the $\epsilon \to 0$ limit, and using the last equation in (25), we obtain that

$$
\int_{\text{Int}(\Gamma_0)} Q \, dV = 0
$$

must hold for the compact streamline Γ_0 of $\mathbf{u}(\mathbf{x})$. The closed curve Γ_ϵ is an attractor if the areas of closed streamlines of $\mathbf{u}(\mathbf{x})$ inside Γ_0 increase under the flow of the inertial equation, and the areas of closed streamlines of $\mathbf{u}(\mathbf{x})$ outside Γ_0 decrease under the flow of the inertial equation. This is the case (by (26)) if

$$
\int_{\text{Int}(\Gamma_-)} Q \, dV > 0 > \int_{\text{Int}(\Gamma_+)} Q \, dV
$$

for all closed streamlines Γ_- and Γ_+ of $\mathbf{u}(\mathbf{x})$ that are close enough to Γ_0 and satisfy $\text{Int}(\Gamma_-) \subset \text{Int}(\Gamma_0) \subset \text{Int}(\Gamma_+)$. This proves formula (16).

Assume now that Γ_ϵ is a nondegenerate (i.e., exponentially attracting or repelling) limit cycle of the inertial equation. We recall from Haller and Iacono [10] that in coordinates tangent and normal to Γ_ϵ, the fundamental matrix solution for the linearized flow along Γ_ϵ can be written as

$$\boldsymbol{\Psi}(t, t_0) = \begin{pmatrix} e^{\int_{t_0}^t S_\parallel(\tau)\mathrm{d}\tau} & \int_{t_0}^t e^{\int_s^t S_\parallel(\tau)\mathrm{d}\tau} e^{\int_{t_0}^s [-S_\parallel(\tau)+\delta(\tau)]\mathrm{d}\tau} a(s)\mathrm{d}s \\ 0 & e^{\int_{t_0}^t [-S_\parallel(\tau)+\delta(\tau)]\mathrm{d}\tau} \end{pmatrix},$$

(27)

where

$$\mathbf{v} = \mathbf{u} + \epsilon \left(\frac{3R}{2} - 1 \right) \left[\frac{D\mathbf{u}}{Dt} - \mathbf{g} \right] + \mathcal{O}(\epsilon^2),$$ (28)

$$S_\parallel = \frac{1}{2} \frac{\left(\mathbf{v}, \left[\nabla\mathbf{v} + (\nabla\mathbf{v})^T \right] \mathbf{v} \right)}{|\mathbf{v}|^2} \Bigg|_{\mathbf{x}=\mathbf{x}(t,\mathbf{x}_0)},$$

$$\delta(t) = \nabla \cdot \mathbf{v}|_{\mathbf{x}=\mathbf{x}(t,\mathbf{x}_0)},$$

with $\mathbf{x}(t, \mathbf{x}_0)$ denoting a T-periodic solution on Γ_ϵ. As shown in Haller and Iacono [10], the parallel strain rate $S_\parallel$ satisfies

$$\int_0^T S_\parallel(t)\mathrm{d}t = 0$$ (29)

along any T-periodic closed orbit of $\mathbf{v}$.

By (27), under one period, infinitesimal perturbations initially orthogonal to Γ_ϵ grow in the direction normal to Γ_ϵ by the factor

$$e^{\int_0^T [-S_\parallel(\tau)+\delta(\tau)]\mathrm{d}\tau} = e^{\int_0^T \delta(t)\mathrm{d}t} = e^{\int_0^T \nabla\cdot\mathbf{v}|_{\mathbf{x}=\mathbf{x}(t,\mathbf{x}_0)}\mathrm{d}t},$$ (30)

where we used (28) and (29). Now, for small ϵ, we can write $\mathbf{x}(t, \mathbf{x}_0) = \bar{\mathbf{x}}(t, \mathbf{x}_0) + \epsilon\hat{\mathbf{x}}(t, \mathbf{x}_0; \epsilon)$ and $T = \bar{T} + \epsilon\hat{T}$ where $\bar{\mathbf{x}}(t, \mathbf{x}_0)$ in an unperturbed periodic solution of period $\bar{T}$ on Γ_0. By (24) and (25), we then have

$$\int_0^T \nabla \cdot \mathbf{v}|_{\mathbf{x}=\mathbf{x}(t,\mathbf{x}_0)}\mathrm{d}t = \int_0^T \nabla \cdot \left[\mathbf{u}(\mathbf{x}) \right.$$

$$\left. + \epsilon \left(\frac{3R}{2} - 1 \right) \frac{D\mathbf{u}(\mathbf{x})}{Dt} + \mathcal{O}(\epsilon^2) \right]_{\mathbf{x}=\mathbf{x}(t,\mathbf{x}_0)} \mathrm{d}t$$

$$= \epsilon \left(\frac{3R}{2} - 1 \right) \int_0^T \nabla \cdot \left[\frac{D\mathbf{u}(\mathbf{x})}{Dt} \right]_{\mathbf{x}=\mathbf{x}(t,\mathbf{x}_0)} \mathrm{d}t + \mathcal{O}(\epsilon^2)$$

$$= \epsilon (2 - 3R) \int_0^T Q(\mathbf{x}(t, \mathbf{x}_0)) \mathrm{d}t + \mathcal{O}(\epsilon^2)$$

$$= \epsilon (2 - 3R) \int_0^{\bar{T}} Q(\bar{\mathbf{x}}(t, \mathbf{x}_0)) \mathrm{d}t + \mathcal{O}(\epsilon^2).$$ (31)

Since the arclength s along the closed streamline Γ_0 satisfies $\mathrm{d}s/\mathrm{d}t = |\mathbf{u}(\bar{\mathbf{x}}(t))|$, we finally obtain from (31) the relation

$$\int_0^T \nabla \cdot \mathbf{v}|_{\mathbf{x}=\mathbf{x}(t,\mathbf{x}_0)}\mathrm{d}t = \epsilon \int_{\Gamma_0} \frac{(2-3R)Q}{|\mathbf{u}|}\mathrm{d}s + \mathcal{O}(\epsilon^2).$$ (32)

We conclude that by (30) and (32), the stability of Γ_ϵ is determined by the integral

$$I(\Gamma_0) = \int_{\Gamma_0} \frac{(2-3R)Q}{|\mathbf{u}|}\mathrm{d}s$$

along Γ_0 for small enough ϵ. Specifically, Γ_ϵ is attracting for $I(\Gamma_0) < 0$, which proves formula (17), and hence completes the proof of (i) of Theorem 3.

A.3.2. Bubbles

Based on our earlier discussion on fixed points, bubbles will either cluster around center-type fixed points of $\mathbf{u}(\mathbf{x})$, or around a closed curve Γ_ϵ that is $\mathcal{O}(\epsilon)$ C^1-close to a closed streamline Γ_0 of $\mathbf{u}(\mathbf{x})$. Repeating the above proof for bubbles ($2 - 3R < 0$), we obtain statement (ii) of Theorem 3.

A.3.3. Neutrally buoyant particles

Neutrally buoyant particle dynamics on the slow manifold is governed by the area-preserving inertial equation $\dot{\mathbf{x}} = \mathbf{u}(\mathbf{x})$. Therefore, typical neutrally buoyant particles will not converge to fixed points or limit cycles; rather, for small enough $\epsilon > 0$, such particles will approach streamlines of $\mathbf{u}(\mathbf{x})$ exponentially fast. This proves statement (iii) of Theorem 3.

References

[1] V. Akcelik, G. Biros, O. Ghattas, K. Long, B. van Bloemen Waanders, A variational finite element method for source inversion for convective–diffusive transport, Finite Elem. Anal. Des. 39 (2003) 683–705.
[2] A. Babiano, J.H.E. Cartwright, O. Piro, A. Provenzale, Dynamics of a small neutrally buoyant sphere in a fluid and targeting in Hamiltonian systems, Phys. Rev. Lett. 84 (2000) 5764–5767.
[3] A.E. Badia, T. Ha-Duong, A. Hamdi, Identification of a point source in a linear advection–dispersion–reaction equation: Application to a pollution source problem, Inverse Problems 21 (2005) 1121–1136.
[4] C. Basdevant, T. Philipovitch, On the validity of the "Weiss criterion" in two-dimensional turbulence, Physica D 73 (1994) 17–30.
[5] I.J. Benczik, Z. Toroczkai, T. Tél, Selective sensitivity of open chaotic flows on inertial tracer advection: Catching particles with a stick, Phys. Rev. Lett. 89/16 (2002) 164501(4).
[6] F. Boano, R. Revelli, L. Ridolfi, Source identification in river pollution problems: A geostatistical approach, Water Resources Res. 41 (2005) W07023.
[7] T.J. Burns, R.W. Davis, E.F. Moore, A perturbation study of particle dynamics in a plane wake flow, J. Fluid Mech. 384 (1999) 1–26.
[8] N. Fenichel, Geometric singular perturbation theory for ordinary differential equations, J. Differential Equations 31 (1979) 51–98.
[9] G. Haller, G. Yuan, Lagrangian coherent structures and mixing in two-dimensional turbulence, Physica D 147 (2000) 352–370.
[10] G. Haller, R. Iacono, Stretching, alignment, and shear in slowly varying velocity fields, Phys. Rev. E 68 (2003) 056304.
[11] F. Katopodes Chow, B. Kosovic, S.T. Chaan, Source inversion for contaminant plume dispersion in urban environments using building-resolving simulations, in: Proc. of 86th American Meteorological Society Annual Meeting, Atlanta, GA, 2006.
[12] C. Jung, T. Tél, E. Ziemniak, Application of scattering chaos to particle transport in a hydrodynamical flow, Chaos 3 (1993) 555–568.
[13] M.R. Maxey, J.J. Riley, Equation of motion for a small rigid sphere in a nonuniform flow, Phys. Fluids 26 (1983) 883–889.
[14] E.E. Michaelides, The transient equation of motion for particles, bubbles, and droplets, J. Fluids Eng. 119 (1997) 233–247.
[15] E. Mograbi, E. Bar-Ziv, On the asymptotic solution of the Maxey–Riley equation, Phys. Fluids 18 (2006) 051704.

[16] A. Okubo, Horizontal dispersion of floatable trajectories in the vicinity of velocity singularities such as convergencies, Deep-Sea Res. 17 (1970) 445–454.

[17] J. Rubin, C.K.R.T. Jones, M. Maxey, Settling and asymptotic motion of aerosol particles in a cellular flow field, J. Nonlinear Sci. 5 (1995) 337–358.

[18] T. Sapsis, G. Haller, Instabilities in the dynamics of neutrally buoyant particles, Phys. Fluids (2007) (submitted for publication).

[19] J. Weiss, The dynamics of enstrophy transfer in 2-dimensional hydrodynamics, Physica D 48 (1991) 273–294.

[20] R.D. Vilela, A.P.S. de Moura, C. Grebogi, Finite-size effects on open chaotic advection, Phys. Rev. E 73 (2006) 026302.